Arch. Metall. Mater. **66** (2021), 2, 397-405

DOI: 10.24425/amm.2021.135871

AMIR BAGHANI[1], ALI KHEIRABI[2*], AHMAD BAHMANI[3], HAMID KHALILPOUR[4]

REDUCING MELT SURFACE TURBULENCE BY EMPLOYING SURGE AND FILTER IN A CONVENTIONAL NON-PRESSURIZING GATING SYSTEM: SIMULATION AND EXPERIMENT

Tensile strength of aluminum castings has been improved by employing surge and filter in a conventional non-pressurizing gating system. For this purpose, three non-pressurizing bottom-gating systems were designed where the first design was a simple design with no filter and no surge, in the second design filter and in the third one surge was added to the end of runner. Tensile strength, Weibull module, scanning electron microscopy, chemical analysis, and melt pattern during the mold filling were thoroughly analyzed to compare these three designs. It was observed that employing filter and surge in the gating system reduces flow kinetic energy and consequently avoid surface turbulence and air entrainment, which leads to castings with fewer defects and higher reliabilities. Finally, it found that appropriate use of surge in the running system can be as effective as employing a filter in reducing melt front velocity.

Keywords: Aluminum casting, filter, surge, oxide bifilms, failure analysis, Weibull module, and mold filling simulation

1. Introduction

Most of the casting defects such as air entrainments, oxide folding, and bifilms are created during the pouring process and deteriorate the mechanical properties [1-3]. Oxide bifilms are formed as a result of turbulent flow and are notorious for their effects on the reduction of tensile strength and deterioration of fatigue properties [4-10]. These defects have been observed even in low pressure die casting (LPDC) productions which expected to have the most laminar flow pattern and controlled free surface [11-15].

Moreover, bifilms expedite nucleation of other defects such as hydrogen pores [16,17] and Fe-rich phases [18]. Campbell [19] introduced a critical velocity value to relate melt velocity to the bifilms folding and entrapment and achieved a critical value of 0.5 m/s for liquid aluminum. Exceeding melt front velocity from this critical value intensifies surface turbulence and triggers severe rates of oxides entrainment.

In order to control or diminish the melt velocity during the pouring process ceramic foam filter is suggested in the gating system. For instance, Nyahumwa [4] used two bottom gating systems for casting of Al-7Si-Mg, one without filter and the second one by embedding a filter at the bottom of sprue. It was observed that the fatigue life for filtered samples, with laminar flow pattern, were six times greater than the one without the filter. Using ceramic filter also reduces the velocity of the melt in a naturally pressurized gating system [20]. In addition, Eisaabadi et al. [21] found that increasing the runner height after the filter over 1.25 cm generates bifilms.

Besides filter, the design and type of the gating system play an important role in decreasing surface turbulence and diminishing the above-mentioned defects [22-28]. In this regard, Shahmiri and Kharrazi [29] have observed that the bottom gating system makes less porosity and decreases the oxide film folding in comparison to the side and top gated systems. Furthermore, a diffusing runner system can decrease the velocity of liquid metal under critical velocity (0.5 m/s for aluminum), while keeping the flow rate unchanged [30].

Traditionally, non-pressurized bottom gating system has been always suggested to provide a laminar flow during the pouring. In this type of gating system, in order to reduce the melt velocity, the cross-section area of the gating system is increased from the sprue to the ingates [31-33].

[1] UNIVERSITY OF IOWA DEPARTMENT OF MECHANICAL ENGINEERING, IOWA CITY, IA, USA
[2] IRAN UNIVERSITY OF SCIENCE AND TECHNOLOGY SCHOOL OF METALLURGY AND MATERIALS ENGINEERING, TEHRAN, IRAN
[3] UNIVERSITY OF TEHRAN DEPARTMENT OF METALLURGICAL AND MATERIALS ENGINEERING, IRAN
[4] LAVAL UNIVERSITY, DEPARTMENT OF MINING, METALLURGICAL AND MATERIALS ENGINEERING, QUÉBEC, CANADA

* Corresponding author: alikheirabi@gmail.com

To describe this phenomenon, the mass conservation for a control volume which has *i* entrance and exit can be presented as follows [34]:

$$\int_{cv} \frac{\partial \rho}{\partial t} dv + \sum_i (\rho_i v_i A_i)_{out} - \sum_i (\rho_i v_i A_i)_{in} = 0 \quad (1)$$

For an incompressible steady flow the first term on the left hand side is canceled and it can be rearranged as follows:

$$\sum_i (\rho_i v_i A_i)_{in} = \sum_i (\rho_i v_i A_i)_{out} \quad (2)$$

Where in the above equation ρ, v, A are density, velocity and cross section area respectively. Subscripts *i*, *out* and *in* stand for channel number, exit flow and entrance flow. According to this equation, assuming that the channel is filled by the fluid completely, increasing the channel area reduces the flow velocity. That's the reason that why non-pressurized gating system always have been recommended.

However, in a recent study by Baghani et al. [35] it determined that even in non-pressurized gating system liquid metals doesn't fill the entire ingate area completely while entering into the mold cavity. This incomplete filing of the ingate is related to the formation of vortex flow and dead zone at the runner extension which pushes the new entry liquid metal into the mold cavity [36]. Therefore, in this condition melt front velocity is not strictly influenced by the ingate cross section area. Finally, they concluded that the conventional calculations and designs for non-pressurized gating system are not accurate enough. Nonetheless, keeping ingate completely filled with melt during the pouring process has never been investigated precisely before.

As mentioned, using filter in the gating system not only decrease the melt velocity but also have the benefits of trapping slags, inclusions and oxide layers. Nonetheless, the use of filter in the gating system is not recommended for production of heavy section castings or because of some technological difficulties. In these situations, using a surge is suggested to decrease the melt initial pressure and trap dirt and inclusions. The aim of this study is to investigate quantitatively the effects of surge on entrapping external dirt, reducing surface turbulence in the running system and compare it with filtered samples and castings without any filter and surge. In this study, mechanical tests, optical microscopy, scanning electron microscopy (SEM) and numerical simulation were used to investigate effects of the filter and surge on the quality of aluminum casting components.

2. Method and procedure

Three designs and models used in this study are presented in Fig. 1. The model 1 was a simple design without filter and

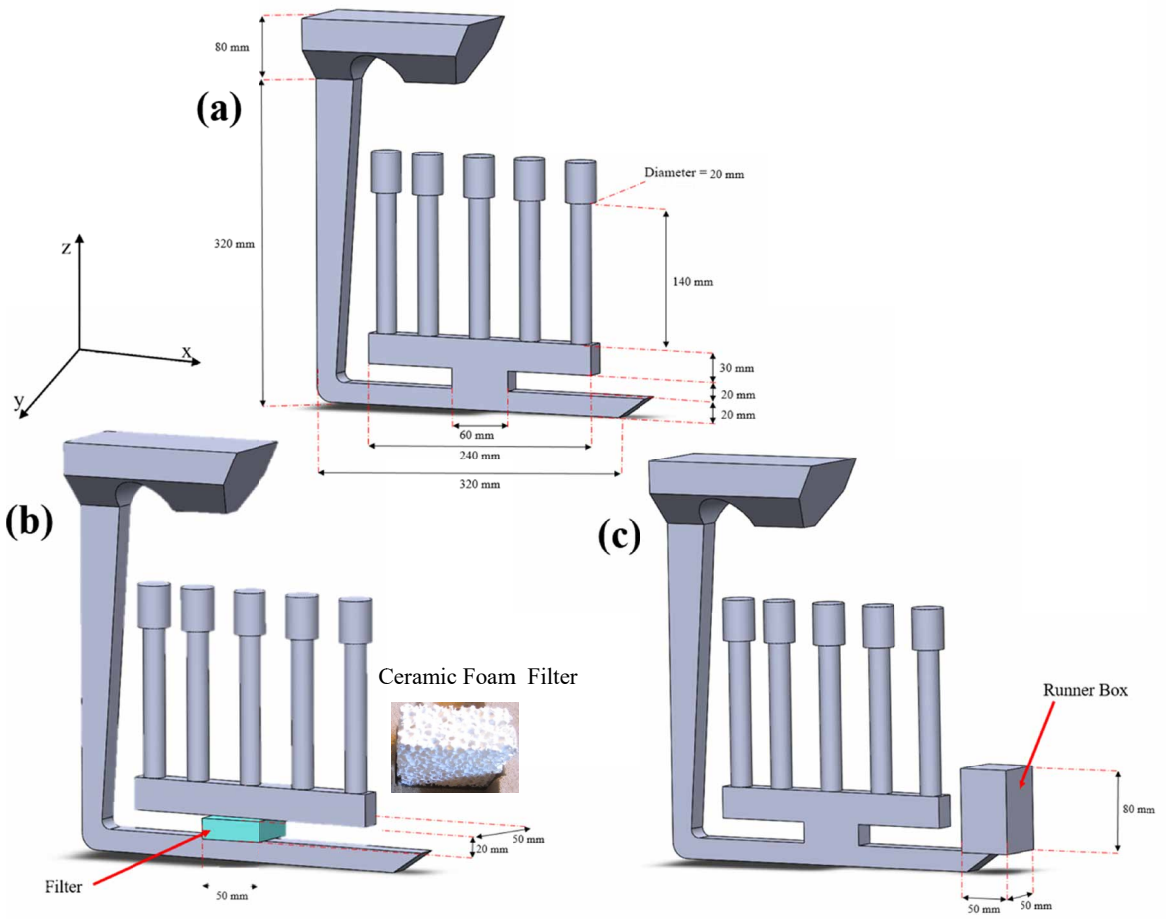

Fig. 1. Three different models used in this study, (a) model 1-Basic design (without filter and surge), (b) model 2-with filter and (c) model 3-with surge (Dimensions are in mm)

surge. A 10 ppi filter and a surge were included in models 2 and 3 respectively (see Fig. 1b and c) while all other dimensions of gating system and casting kept the same. Each model contained five sample bars, each with a diameter of 20 mm and length of 140 mm, which were used for preparation of tensile test samples. Cold box method employed for molding process including mixture of dry silica sand and sodium silicate binder which cure by blowing CO_2 gas. The mold area above each cylindrical sample were drilled to make vent and let the gases leave the mold. In this study, commercial aluminum A356 ingot were melted in an electrical resistance melting furnace and its chemical composition was analyzed after the melting by the optical emission spectroscopy (Table 1). Argon inert gas were used to protect the melt surface.

TABLE 1

Chemical composition of aluminum melt in weight percent

Al	Si	Mg	Fe
Base	7.4	0.2	0.3

Nitrogen inert gas was used to remove hydrogen dissolved in the melt at 750°C for 3min, and then melt poured at 720°C into the sand mold (Fig. 2). To ensure the quality of castings and to collect more data each model was molded and poured two times. All three designs have presented in Fig. 3 after the shake out.

The casting specimens were machined according to the British Standard of BS EN 10002-1: 2002 [BSI 2001], to obtain dimensions of 6.75 mm diameter and 25 mm gauge length on a 40 mm parallel length. Tensile testing was carried out with an Instron 1195-5500R machine with a cross-head speed of 1 mm/min. The ultimate tensile strength (UTS) values were analyzed using a two-parameter Weibull distribution to evaluate the distribution of the mechanical properties:

$$p_i = 1 - \exp\left[-\left(\frac{\sigma_{UTS}}{\sigma_0}\right)^m\right] \tag{3}$$

Where p_i is the failure probability and the fraction of samples failed at or below a measured value of ultimate tensile strength σ_{OUT}. In this equation σ_0 is a characteristic value of ultimate tensile strength σ_{OUT} at which 62.8% of all of the specimens have failed, and finally, m is the Weibull modulus. The failure probability p_i can be calculated from the following formula $p_i = \frac{i-a}{N+b}$, where a and b are given numbers between 0 and 1.

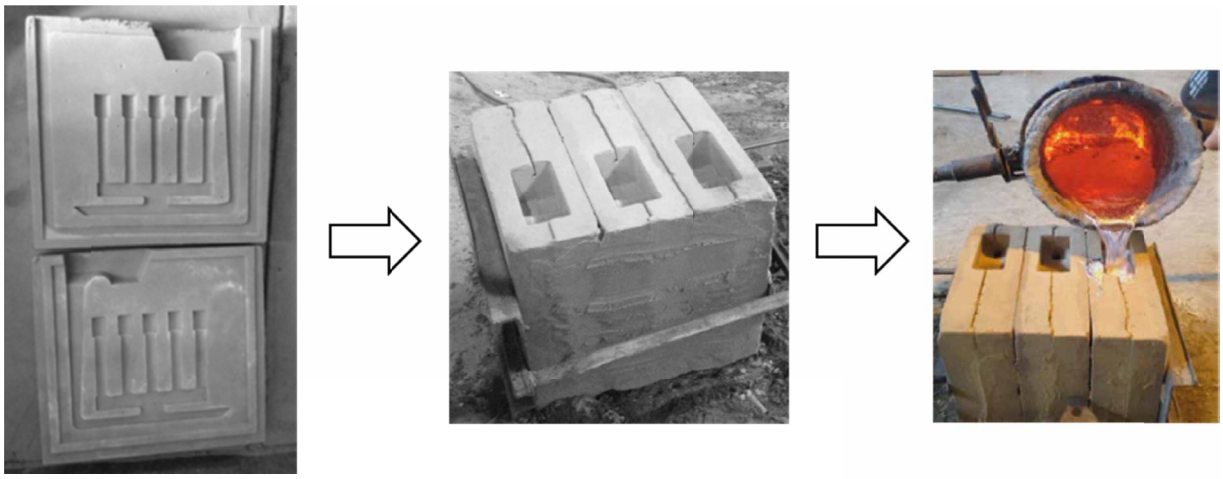

(a) (b) (c)

Fig. 2. Molding and pouring process (a) mold right and left halves (b) mold assembly and (c) pouring aluminum melt

(a) Model 1 (basic design) (b) Model 2 (with filter) (c) Model 3 (with surge)

Fig. 3. Presentation of gating system and casting samples after shake out, (a) model 1-basic design, (b) model 2-with filter and (c) model 3-with surge

In this study, both numbers were set equal to zero. Equation 3 can be rearranged as follows:

$$\ln\left[\ln\left(\frac{1}{1-p_i}\right)\right] = m\cdot\ln\left(\sigma_{UTS}\right) - m\cdot\ln\left(\sigma_0\right) \qquad (4)$$

The equation 4 is presented in a linear form of $y = mx + c$ where m is the slope of the line presents the Weibull modulus that is a single value explaining the distribution of properties. In particular, a higher Weibull modulus means a narrower distribution of properties which indicates that produced casting components have a lower amount of defects and higher reliability [37,38].

The fracture surfaces of the tensile test sample bars were analyzed using a scanning electron microscopy (SEM) and energy dispersive spectroscopy (EDS) analyzer linked to the SEM. Optical microscopy was used to investigate the distribution of defects near the fracture surfaces.

In order to study the flow pattern of three different desgins, ProCAST a commercial FEA package for metal casting simulation was used to model the transient mold filling process. Three simulations for three models of 1, 2 and 3 were run by applying the atmospheric pressure on the top of the pouring basin cup to study the distribution of velocity and mold filling pattern. For all these simulations, no-slip boundary condition, which assumes no movement for the flow on the mold surface, was applied at the interface of melt and mold walls. In model-2, a cubical region which connects the runner to the mold cavity has been categorized as a 10 ppi ceramic filter. Once the liquid metal reaches to this filter area, the Forchheimer equation is solved to model the flow in porous area. This equation will be explained in more details later in the discussion section. In all simulations, pouring temperature of 720°C, initial pouring height of 80 mm and ambient temperature of 28 °C were considered. In addition, dry silica sand and AlSi7Mg were selected as mold and cast material where the details of thermal properties can be found in Table 2. Since the focus of this study is on the melt flow pattern during mold filling, solidification and cooling simulations was ignored.

Tetrahedral linear mesh generation produced 120000, 120095 and 120635 fluid cavity meshes for model-1, model-2 and model-3 respectively. The longest simulation duration, CPU time, was reported 3.75 hours for the model-3 with surge with a computational system configuration of Corei5, 8GB RAM.

3. Results

Table 3 shows the results of UTS obtained from the tensile tests at room temperature for the three models (column 1 is the closest to the sprue). The average UTS of samples revealed that the tensile strength in model 1 (114.56 MPa) is lower than either model 2 (162.85 MPa) and model 3 (150.52 MPa). It means that tensile properties have been increased 40% and 29.8% in model 2 and model 3, respectively. The UTS range of distribution in model 1, 2 and 3 was 51 MPa, 10 MPa and 19 MPa respectively.

The variation of average UTS with column number for all three models are presented in Fig. 4. It was observed that the

TABLE 2

Thermo-physical properties of aluminum casting and silica sand mold

	Thermal conductivity ($W\cdot m^{-1}\cdot K^{-1}$)	Density ($Kg\cdot m^{-3}$)	Specific Heat ($J\cdot Kg^{-1}\cdot K^{-1}$)	Liquidus Temperature (°C)	Latent Heat ($KJ\cdot Kg^{-1}$)
Aluminum	70	2410	1150	613	430
Silica Sand	0.7	1520	1167	—	—

TABLE 3

Ultimate tensile strength (MPa) of sample bars for three different design

Model	Column No.	Pouring Trial 1	Pouring Trial 2	Column average	Total average
Model 1 (basic design)	1	—	102.35	102.35	114.56±51
	2	130.41	137.10	133.75±3.34	
	3	110.22	121.34	115.78±5.56	
	4	132.51	132.44	132.47±0.03	
	5	86.45	90.50	88.47±2.025	
Model 2 (with filter)	1	160.17	160.10	160.13±0.035	162.85±10
	2	163.14	162.23	162.68±0.455	
	3	162.5	161.30	161.90±0.6	
	4	162.22	162.01	162.11±0.105	
	5	170.11	164.81	167.46±2.65	
Model 3 (with surge)	1	146.43	145.90	146.16±0.265	150.52±19
	2	148.72	148.00	148.36±0.36	
	3	141.44	144.10	142.77±1.33	
	4	160.32	158.00	159.16±1.16	
	5	157.84	154.54	156.19±1.65	

magnitude of tensile stress in model 2 is greater than the one for Model 3 and significantly greater than the one for model 1. In model 1, UTS values are oscillating with column number while in model 2 and 3 no sharp variation in data was observed.

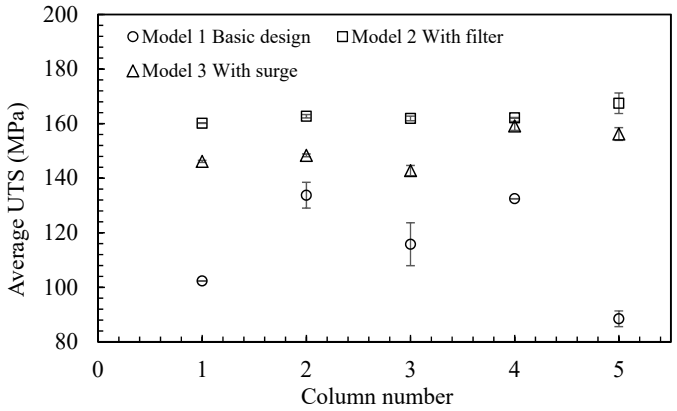

Fig. 4. Ultimate tensile strength of sample bars with column number

Distribution of the Weibull parameter is depicted in Fig. 5 where the x-axis presents the natural logarithm of UTS for three different models. It shows that the distribution range of UTS for the model 1 is five times greater than the one for the model 2 and 3.

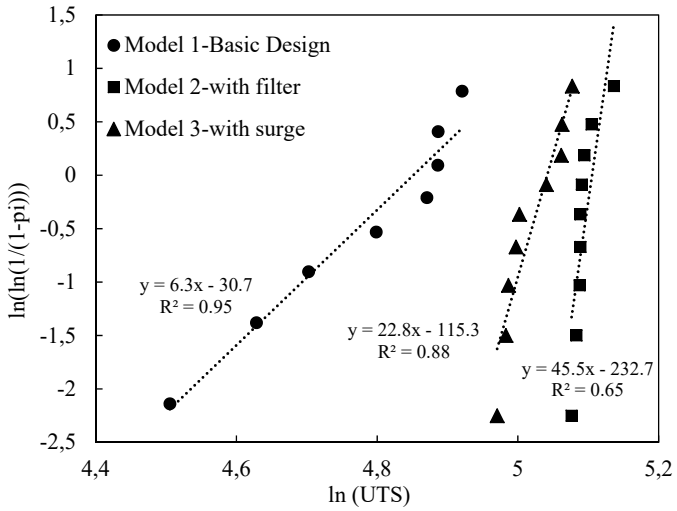

Fig. 5. Weibull distribution for three models

The slopes of the fitted lines, the Weibull modulus, for models 1, 2 and 3 are 6.3, 45.5 and 22.8 respectively. In fact, models using filter and surge show narrower distribution of tensile strength in comparison with the basic model without filter and surge. Therefore, it is expected to see fewer defects in models 2 and 3.

The optical microscopy of three models is shown in Fig. 6 where model 1 contains several macroscopic inclusions and impurities while no bubble and inclusion was observed in model 2 with filter and a few inclusions were found in model 3 with the surge. It is worth mentioning that the same melt was used for pouring of all samples.

Images of scanning electron microscopy of the fracture surfaces of tensile test samples are illustrated in Fig. 7 for the three models. Oxide bifilms, shrinkage porosity and gas bubble were easily observed on the fracture surfaces of samples belonging to the model 1 (Fig. 7a). EDS analysis of point 1in Fig. 7a proves the existence of oxide layer. On the other hand, in model 2 (Fig. 7b), on the fracture surfaces of the samples no shrinkage, inclusion and gas porosity were found. Similarly, in model 3, based on our observations only one location with shrinkage porosity was detected on the fracture surface of one of the samples (Fig. 7c). Intergranular and transgranular brittle fracture are the dominant fracture mechanisms in model 2 and 3, while in model 1 initial cracks were initiated from biflms, shrinkages and gas porosities.

Distribution of z-direction (direction of down srpue) velocities, at the moment that the liquid metal is entering into the mold cavity, is presented in Fig. 8. As it can be seen, the melt in Model 1 and 2 have the highest and lowest velocities, respectively. The melt front velocity in Model 1 is around 2 m/s, which is far above the critical value of 0.4-0.6 m/s for aluminum alloys [19]. On the other hand, keeping the entrance velocity under 0.2 m/s and having smooth flow pattern is obtained using a filter in Model 2. The remarkable result to emerge from the fluid flow simulation is that flow in model 3 with a surge at the runner extension, is not as smooth as Model 2, but present a more laminar regime in comparison with Model 1.

Z-direction velocities have been quantitatively compared for three models along line 1 located in the ingate, (Fig. 9). These velocity values were extracted for each model, right at the moment that the melt is entering into the mold cavity. The most

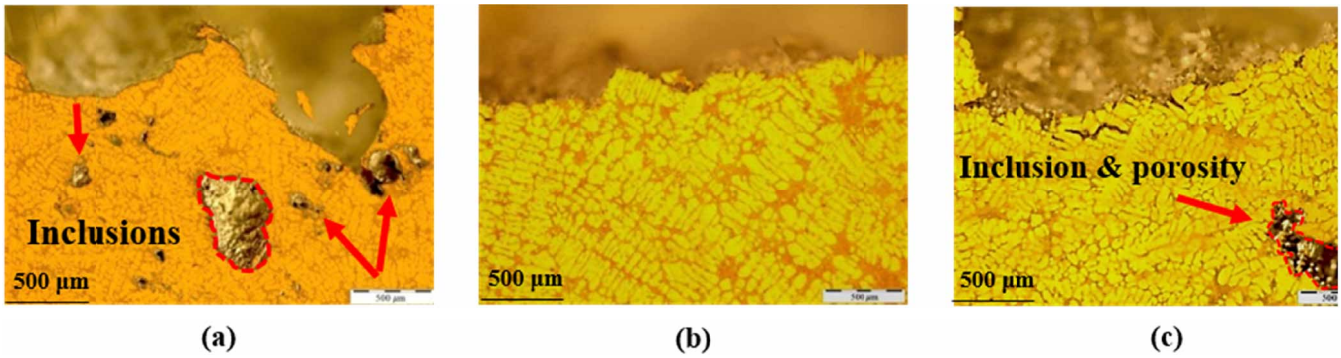

Fig. 6. Optical microscopy of tensile test fracture subsurface (a) model 1-Basic design, (b) model 2-with filter and (c) model 3-with surge

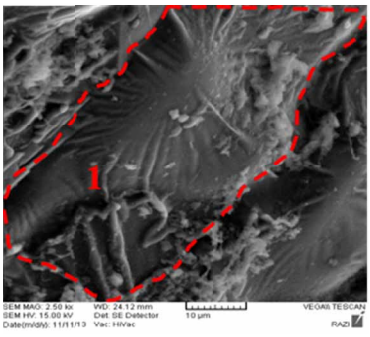

Oxide films

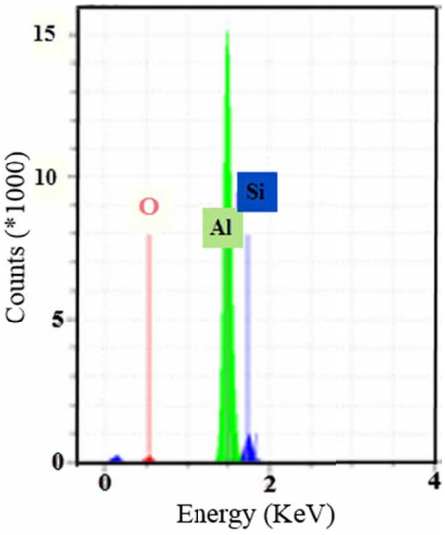

EDS analysis of point 1

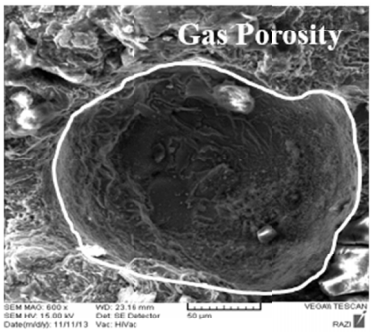

Gas porosity

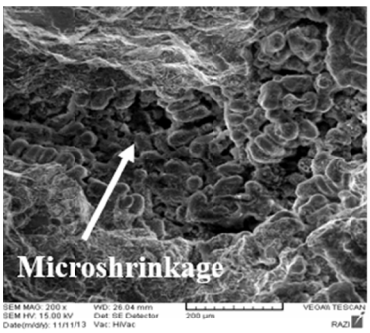

Shrinkage porosity

(a) Model 1 (basic design)

(b) Model 2 (with filter)

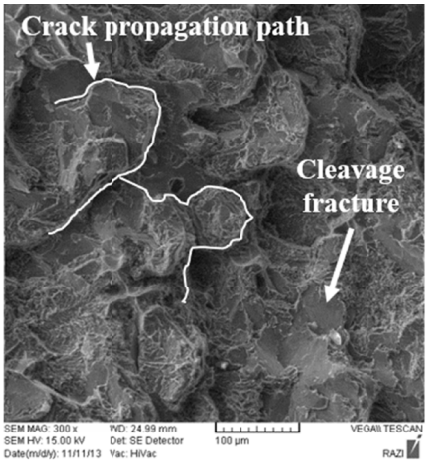

Intergranular brittle fracture

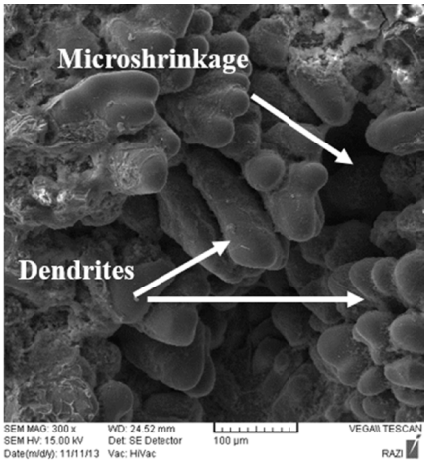

Shrinkage porosity

(c) Model 3 (with surge)

Fig. 7. Scanning electron microscopy images of fracture surfaces of the tensile test bars obtained from (a) model 1-Basic design, (b) model 2-with filter and (c) model 3-with surge

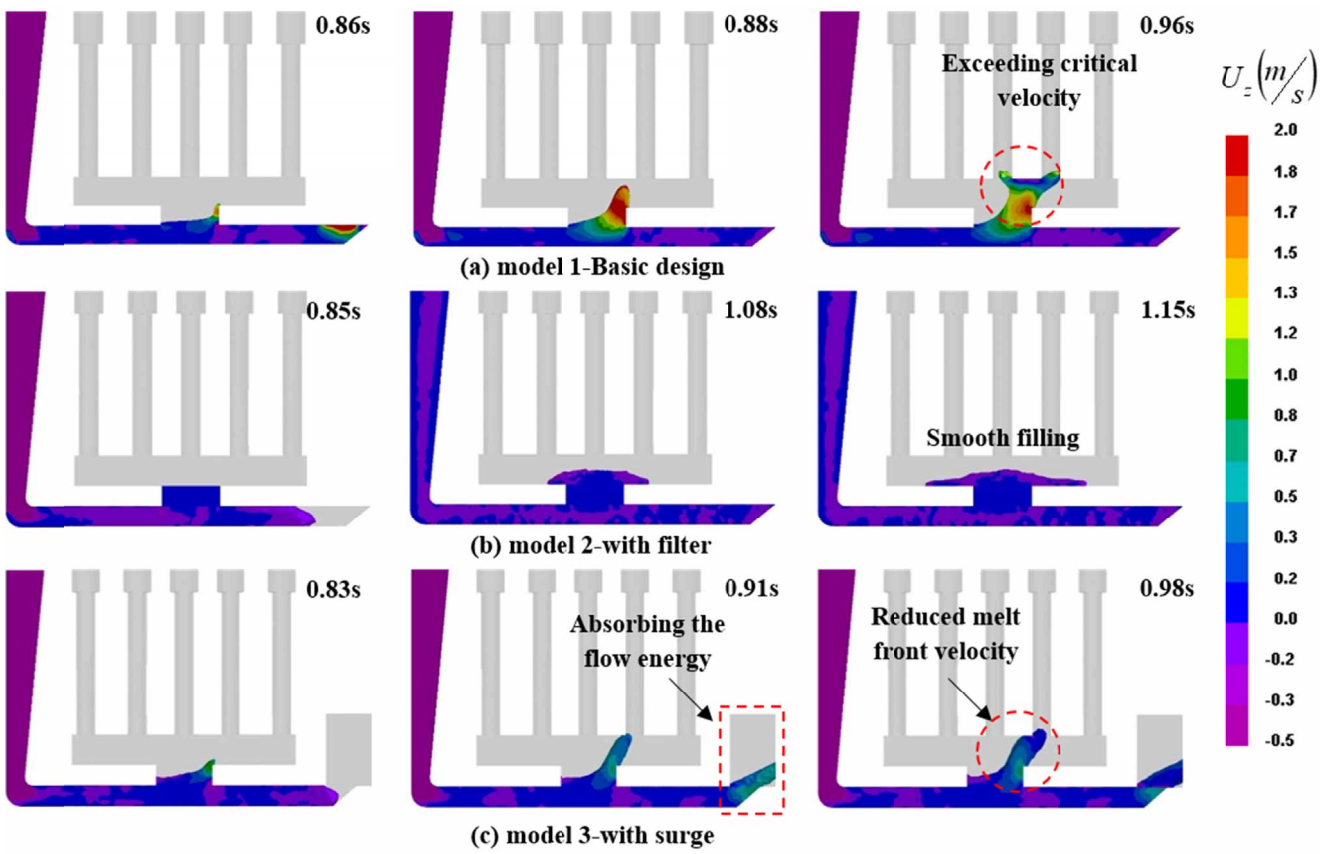

Fig. 8. Distribution of z-direction velocity while the liquid metal is filling the gating system and entering into the mold cavity in (a) model 1-Basic design, (b) model 2-with filter and (c) model 3-with surge

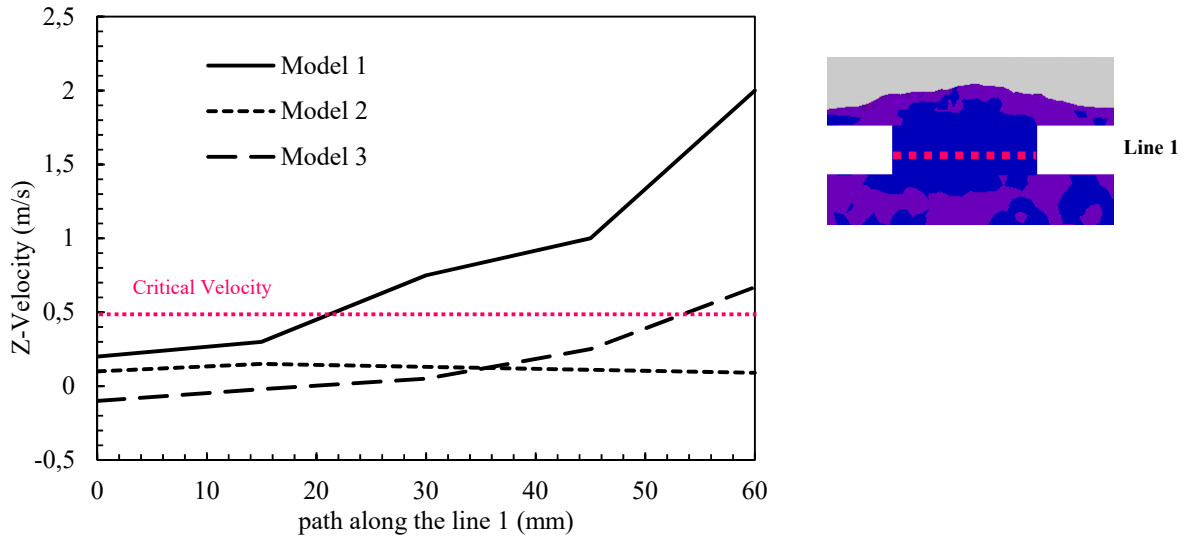

Fig. 9. Comparison in z-direction velocities (vertical velocity) along line 1, in model 1-Basic design, model 2-with filter and model 3-with surge

uniform, smooth and laminar flow belongs to the model 2 which uses a filter in the ingate. In model 2, melt front shape is flat, doesn't exhibit disturbed surface and its velocity is less than the critical value of 0.5 m/s. The maximum velocity in models 1, on the right side of the ingate, is 2 m/s which is more than the one for model 3 (0.65 m/s). These results show that using a surge at the end of the runner will successfully decrease the front velocity during the filling process.

4. Discussion

In order to investigate the effects of filter and surge on mechanical properties of the aluminum casting, three models of 1, 2 and 3 poured two times and ten tensile test specimens for each model were prepared for tensile tests and then fractography. The results of this study clearly indicate that using surge (model 3) in the gating system improve the mechanical properties and reli-

ability of aluminum castings. Samples produced by embedding a filter in gating system (model 2) still present best mechanical properties, but it is possible to reach the same properties by employing surge in the gating system.

Average ultimate tensile strength of model 2 and 3 are very close, and are significantly higher than the one for model 1. It was also observed in model 1 ultimate tensile strength is oscillating with column number which is a sign of arbitrary distribution of defects in this model. In fact, ceramic foam filter and surge in the gating system decrease the melt front velocity, at the moment that the melt enters into the mold cavity.

The primary effect of using filters in the ingate system is to decrease the melt velocity and ensure that the ingate system is fully filled before the melt enters the gates. Filter decreases the melt velocity, and an increase in back pressure will fill the sprue by the liquid metal. An early filling of the sprue prevents the melt from entraining oxide films [20,21,39,40].

The Forchheimer equation describes the pressure drop after the filter for the Newtonian and incompressible fluids as follows [41]:

$$\frac{\Delta p}{L} = \frac{\mu}{k}u + \frac{\rho C_f}{k^{0.5}}u^2 \qquad (5)$$

Where Δp, L, μ, k, u, ρ and C_f are pressure drop, filter length, viscosity, filter permeability, fluid velocity and density and inertia coefficient respectively. This term is added to the right hand side of the momentum equation and for the portion of liquid metal that filled the filter area this term will be active and non-zero. According to the equation 5, pressure drop increases by having higher melt velocity and larger filter with less permeability. This pressure drop then decreases the melt velocity and makes the melt front smooth.

According to our experimental and simulation findings (Figs 6-9), in model 3, surge entraps the inclusions and oxide layers of poured melt and also absorbs kinetic energy of flow. According to figures 6 and 7, less inclusions and bifilms were found beneath and on the fracture surface. Figure 8c shows that in model-3 the first poured melt, which is contain inclusions and bifilms, fills the runner and then is entrapped inside the surge at the end of runner. Figure 9 presents that the melt in model-3 with surge fills the ingate and mold cavity with less melt front velocity compare to the model-1. This reduce the possibility of oxide films separation, folding and entrapment in model-3. As mentioned earlier, bifilms are appropriate sites for nucleation of other defects such as shrinkage and gas porosity which cause to decrease the mechanical properties of aluminum casting components remarkably [4-10,42,43].

Study of Weibull analysis provides considerable insight into a wider distribution of UTS in model 1 in comparison with two other models. This finding can be a sign of entrapped bifilms inside the casting samples which increase the uncertainty of the casting properties. In fact, higher Weibull modulus means a narrower distribution of UTS which shows the fewer amounts of entrapped defects [16-20].

Several shrinkage and gas porosities were found on the fracture surfaces of tensile test samples in model 1 which are the fracture initiation sites. In contrast with model 1, model 2 and model 3 were to some extend defect free and intergranular and transgranular brittle fracture easily observed on the fracture surface. In addition, presence of micro cracks on the fracture surface of samples in model 2 and 3 demonstrates that no other appropriate crack nucleation sites were available in these samples. Moreover, microscopic and macroscopic observations proved that not using filter and surge in the gating system increase the bifilms entrapment inside the cast which act as nucleation sites for crack initiation.

5. Conclusions

Effects of using filter and surge in the gating system on mechanical properties of the aluminum casting were evaluated. It was observed that using filter and surge increase the ultimate tensile strength (UTS) of aluminum casting 40% and 29.8%, respectively. Weibull modulus, in basic model, model with filter and model with surge are 6.3, 45.5 and 22.8 respectively. This means, gating systems with filter and surge exhibit narrower distribution of tensile stresses in comparison with the basic model which doesn't have filter and surge. Moreover, defects such as oxide layer films, shrinkage and gas porosities were found on the fracture surfaces of the tensile test samples belonging to the conventional non-pressurizing gating system without filter and surge. It concluded that the use of surge decreases the melt front velocity and entrap inclusions and oxide layers and eventually improve the mechanical properties of aluminum casting components. By appropriate use of surge in the gating system it is possible to achieve mechanical properties as good as filtered samples.

REFERENCES

[1] C. Reilly, N.R. Green, M.R. Jolly, Appl. Math. Model. **37**, 611-628 (2013).

[2] S.G. Liu, F.Y. Cao, X.Y. Zhao, Y.D. Jia, Z.L. Ning, J.F. Sun, Mat. Sci. Eng. A **626**, 159-164 (2015).

[3] M.A. El-Sayed, H.A. Salem, A.Y. Kandeil, W.D. Griffiths, Metall. Mater. Trans. B **45**, 1398-1406 (2014).

[4] C. Nyahumwa, N.R. Green, J. Campbell, AFS Trans. **106**, 215-223 (1998).

[5] T. Kargul, E. Wielgosz, J. Falkus, Arch. Metall. Mater. **60**, 221-225 (2015).

[6] J. Campbell, N.R. Green, Trans. Amer. Found. Soc. **114**, 341-347 (1994).

[7] M.A. El-Sayed, H. Hassanin, K. Essa, Int. J. Adv. Manuf. Technol. **86**, 1173-1179 (2016).

[8] M.A. El-Sayed, W.D. Griffiths, Int. J. Cast Met. Res. **27**, 282-287 (2014).

[9] J. Campbell, J. Mater. Sci. **51**, 96-106 (2016).
[10] M.H. Ghanaatian, R. Raiszadeh, Mater. Sci. Technol. **33**, 2-8 (2016).
[11] B. Zhang, S.L. Cockcroft, D.M. Maijer, J.D. Zhu, A.B. Phillion, JOM **57**, 36-43 (2005).
[12] P.R. Raju, B. Satyanarayana, K. Ramji, K.S. Babu, Eng. Fail. Anal. **14**, 791-800 (2007).
[13] M. Merlina, G. Timelli, F. Bonollob, G.L. Garagnania, J. Mater. Process. Technol. **209**, 1060-1073 (2009).
[14] L. Sowa, A. Bokota, Arch. Metall. Mater. **57**, 1163-1169 (2012).
[15] E. Omrani, P.L. Menezes, P.K. Rohatgi, Int. J. Eng. Sci. Technol. **19**, 717-736 (2016).
[16] W. Griffiths, R. Raeiszadeh, J. Mater. Sci. **44**, 3402-3407 (2009).
[17] A. Bahmani, N. Hatami, P. Davami, N. Varahram, M. Ostadshabani, J. Adv. Manuf. Tech. **64**, 1313-1321 (2012).
[18] X. Cao, J. Campbell, Metall. Mater. Trans. A **34**, 1409-1420 (2003).
[19] J. Campbell, J. Runyoro, Foundaryman **85**, 117-124 (1992).
[20] H. Hashemi, R. Raiszadeh, J. Appl. Sci. **9**, 2115-2122 (2009).
[21] G. Eisaabadi Bozchaloeia, N. Varahram, P. Davami, S.K. Kim, Mater. Sci Eng. A. **548**, 99-105 (2012).
[22] H. Bagherpoor-Torghabe, B. Niroumand, M. Karbasi, Int. J. Adv. Manuf. Technol. **75**, 677-685 (2014).
[23] A. Anilchandra, L. Arnberg, F. Bonollo, E. Fiorese, G. Timelli, Materials. **10** (9), 1011-1023 (2017).
[24] M.A. El-Sayed, H. Hassanin, K. Essa, Int. J. Cast. Met. Res. **29**, 350-354 (2016).
[25] S.H. Majidi, J. Griffin, C. Beckermann, Metall. Mater. Trans. B **49**, 2599-2610 (2018).
[26] A. Kermanpur, S.H. Mahmoudi, A. Hajipour, J. Mater. Process. Technol. **206**, 62-68 (2008).
[27] M. Prakash, P. Cleary, J. Grandfield, J. Mater. Process. Technol. **209**, 3396-3407 (2009).
[28] A. Sanitas, M. Bedel, M.M. Mansori, J. Mater. Process. Technol. **254**, 124-134 (2018).
[29] M. Shahmiri, Y.H.K. Kharrazi, IJE Trans. B **20**, 155-166 (2007).
[30] F. Hsu, H. Lin, Metal. Mater. Trans. B **40**, 833-842 (2009).
[31] S.I. Karsay, Ductile Iron III: gating and risering, 1981 Quebec Iron and Titanium Corporation.
[32] R.W. Heine, C.R. Loper, P.C. Rosental, Principle of Metal Casting. 1976 Tata McGrow-Hill.
[33] ASM Metals Handbook Volume15, Casting, 2008 ASM International.
[34] Frank White, Fluid Mechanics, 2015 McGraw-Hill Higher Education.
[35] A. Baghani, A. Bahmani, P. Davami, N. Varahram, M. Ostadshabani, Proc. Inst. Mech. Eng. L J. Mater. Des. Appl. **229** (2), 106-1160 (2013).
[36] A. Kheirabi, A. Baghani, A. Bahmani, M. Tamizifar, P. Davami, M. OstadShabani, A. Mazahery, Proc. Inst. Mech. Eng. L J. Mater. Des. Appl. **232** (3), 230-241 (2015).
[37] M. Tiryakioğlu, J. Campbell, J. Inter. Metal cast. **8**, 39-42 (2014).
[38] M. Tiryakioğlu, Metall. Mater. Trans. A **46**, 270-280 (2015).
[39] G. Eisaabadi Bozchaloeia, P. Davami, S.K. Kim, M. Tiryakioğlu, Mater. Sci. Eng. A **579**, 64-70 (2013).
[40] H.Y. Hwang, C.H. Nam, Y.S. Choi, J.H. Hong, X. Sun, China Foundry **14**, 216-225 (2017).
[41] B.V. Antohe, J.L. Lage, D.C. Price, R.M. Weber, ASME. J. Fluids Eng. **119**, 404-412 (1997).
[42] B. Skalerrud, T. Iveland, G. Harkegard, Eng. Fract. Mech. **44**, 857-874 (2003).
[43] J. Campbell, S. Fox, Scripta Mater. **43**, 881-886 (2000).